DOE Final Report

DOE Award number: DE-SC0008799

Recipient of award: Brown University, 164 Angell St., Office of Research Administration, Providence, RI 02912

Title: A Unified Understanding of Residual Stress in Thin Films: Kinetic Models, Experiments and Simulations

Principal Investigator: Eric Chason

Period covered in this progress report: 9/1/2012 – 11/30/2017

Submitted: Feb. 5, 2018

1. Executive summary

Thin films are critical for a wide range of advanced technologies. However, the deposited films often have high levels of residual stress that can limit their performance or lead to failure. The stress is known to depend on many variables, including the processing conditions, type of material, deposition technique and the film's microstructure. The goal of this DOE program was to develop a fundamental understanding of how the different processes that control thin film growth under different conditions can be related to the development of stress.

In the program, systematic experiments were performed or analyzed that related the stress to the processing conditions that were used. Measurements of stress were obtained for films that were grown at different rates, different solutions (for electrodeposition), different particle energies (for sputter deposition) and different microstructures. Based on this data, models were developed to explain the observed dependence on the different parameters. The models were based on considering the balance among different stress-inducing mechanism occurring as the film grows (for both non-energetic and energetic deposition). Comparison of the model predictions with the experiments enabled the kinetic parameters to be determined for different materials. The resulting model equations provide a comprehensive picture of how stress changes with the processing conditions that can be used to optimize the growth of thin films.

2. Background: measurements and modeling of thin film stress

2.1 Measurement of stress using wafer curvature

Our understanding of stress evolution comes from real-time measurements of the stress-induced curvature in the substrate (wafer curvature). In our lab, we use a technique we developed that works by monitoring the deflection of a parallel array of laser beams reflected from the sample surface. The measured curvature (κ) can be related to the average film stress $\bar{\sigma}$ by the Stoney equation [1]:

$$\kappa = \frac{6\bar{\sigma} h_f}{M_s h_s^2} \qquad (1)$$

where h_f is the film thickness, h_s is the substrate thickness and M_s is the biaxial modulus of the substrate. The average stress is calculated by integrating the in-plane stress over the thickness of the film. $\bar{\sigma} h_f$ is often referred to as the stress-thickness.

In a growing film the stress-thickness changes with time as

$$\frac{d(\bar{\sigma}h_f)}{dt} = \sigma(h_f)\frac{\partial h_f}{\partial t} + \int_0^{h_f} \frac{\partial \sigma(z,t)}{\partial t}\, dz \qquad (2)$$

$\sigma(h_f)$ is called the incremental or instantaneous stress; it is the stress being added to the film in the layer at the surface. If the stress in the layers that have already been deposited is not changing (i.e., $\partial\sigma(z,t)/\partial t=0$), the incremental stress is proportional to the change in the stress-thickness with the thickness [2]:

$$\sigma(h_f) = \frac{d(\bar{\sigma}h_f)}{dh} \qquad (3)$$

However, if the stress in the existing layers is changing, e.g., by grain growth, this can lead to additional stress during and after the growth.

2.2 Model of stress during growth without energetic particles

To explain the stress during non-energetic film growth, we developed a kinetic model that incorporates different stress-generating mechanisms into rate equations. To our knowledge, this is the first model that quantitatively connects the stress during deposition to the growth rate, atom mobility, and grain size. The ability to calculate the stress for different conditions allows it to be compared directly with experiments to test its validity.

The stress generation is assumed to occur between adjacent islands at the triple junction at the top of grain boundaries. It is further assumed to be independent of the stress in the other layers [3]. When the grain boundary initially forms, the stress becomes tensile with a value σ_T that depends on the grain size as $L^{-½}$, based on the mechanism proposed by Hoffman [4]. Subsequently, the stress can become less tensile or even compressive because of the diffusion of adatoms from the surface into the triple junction. This is proposed to occur because the chemical potential of adatoms on the surface is raised by the flux of deposited atoms (i.e., supersaturation).

Putting these processes into a rate equation describes how the stress in each layer depends on the growth rate R in the steady-state regime:

$$\sigma_{growth} = \sigma_C + (\sigma_T(L) - \sigma_C)e^{-\frac{\beta D_{eff}}{RL}} \qquad (4)$$

where L is the grain size at the surface and βD_{eff} is a kinetic parameter. The dependence on the parameter $\beta D_{eff}/RL$ represents the balance between the tensile and compressive stress mechanisms at the triple junction [5]. When the film grows fast or the diffusivity is low, the grain boundary formation is rapid relative to the time it takes to insert atoms into the grain boundary and the stress is tensile. When the opposite is true, atoms can diffuse into the triple junction and the stress is compressive. This model has been used to explain stress data in a number of systems [5-12].

3. Results of the research studied in this program

3.1 Transitions in stress vs. thickness using patterned films

In films with relatively high atomic mobility, the stress changes from tensile to compressive as the thickness increases. This behavior has been a long-standing puzzle, but it can be explained within our growth model (eq. 4) by considering how the grain boundary velocity (dh_{gb}/dt) changes as the microstructure evolves during growth. At the initial point of coalescence, the grain boundary grows very

rapidly because of the steep contact angle between the coalescing grains. As the film becomes thicker, the velocity of the grain boundary decreases asymptotically to the average growth rate (R). The dependence of the predicted stress on dh_{gb}/dt shows how this makes the incremental stress less tensile/more compressive with increasing thickness.

Although this is consistent with the observed stress stages, the model is difficult to compare quantitatively with typical film growth experiments since the grain shape is not known. To address this, we have measured stress in films grown on lithographically-patterned substrates so that the film morphology can be controlled. Since electrodeposition makes islands grow with a constant radial growth rate, a 2-d array grows in the form of hemispheres while a 1-d array grows in the form of half-cylinders. An SEM image of the 2-d island morphology is shown in the inset of figure 1.

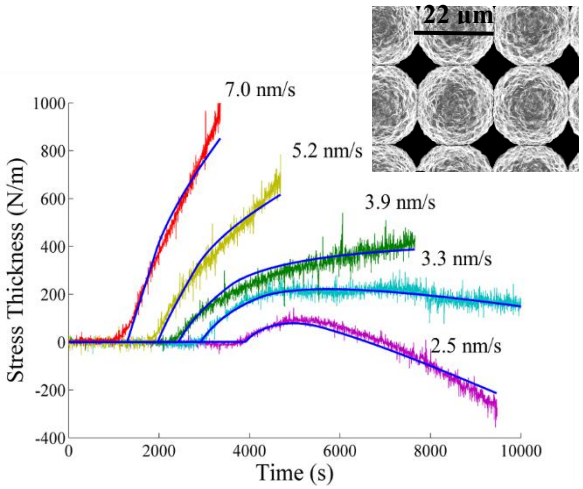

Figure 1. a) b) Stress-thickness evolution for patterned array of Ni islands at growth rates indicated in figure. Solid lines are fit to kinetic model. Inset: SEM micrograph of island array.

Data for the stress-thickness evolution in 2-d island arrays grown at different deposition rates is shown in figure 1 [13]. The known morphology allows us to calculate the stress-thickness evolution for comparison with the experiments. The model calculations are shown as the solid lines in the figure; the parameters for the calculation were obtained by fitting all the data with one set of values for σ_T, σ_C and a small variation in βD_{eff}. The difference between the calculated stress plots is the growth rate. The good agreement supports the model's approach of focusing on the stress at the triple junction.

We have also analyzed the stress evolution in 1-d arrays with different spacings [14]. The calculations from the model for 1-d patterning agree well with the stress-thickness data as a function of both the growth rate and the pattern spacing. Analysis of this work included considering the different rates of grain boundary formation for the different geometries in 1-d (half-cylinders) vs. 2-d (hemispheres).

3.2 Dependence of steady-state stress on growth rate and grain size: effects of kinetics and microstructure

The model predicts a dependence of the steady-state stress on the parameters σ_T, σ_C, βD_{eff}, R and L (eq. 4). These predictions can be tested by fitting the model to steady-state stress data measured under different conditions (e.g., growth rate, temperature). To do this correctly, it is important to also consider the potential effect of the changing grain size during growth. We discuss here how the effect of grain size evolution was accounted for in measurements of electrodeposited Ni and Cu.

The model predicts that changing L changes the incremental stress at the surface. But this has been difficult to study because the effect of grain size at the surface cannot easily be separated from stress due to grain growth below the surface. For some materials such as electrodeposited Ni, there is little grain growth during or after deposition, so this is not a problem. However, for electrodeposited Cu, there is a stronger dependence of L on the thickness. This leads to an increasing grain size at the surface, but can also induce grain growth in the near-surface region. The grain growth does not propagate uniformly through the film so that the grains near the surface are larger than those near the substrate, where the film growth started.

To separate the effects of changing grain size from subsurface grain growth, we used the following measurement strategy. The stress-thickness was measured during growth at one growth rate

until the slope reached a steady-state value to determine the incremental stress. Then the growth was paused in order to allow any subsurface grain growth to occur. When the stress-thickness stopped changing (typically after 2-3 minutes), then the growth was resumed at the same or a different growth rate. The growth was maintained again until the slope reached another steady-state value.

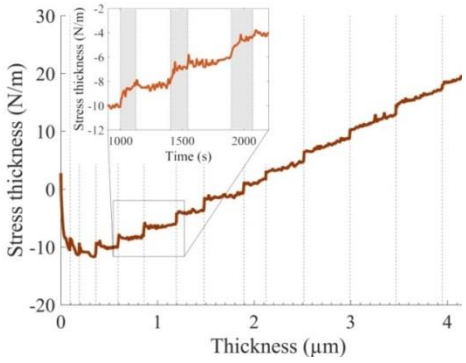

Figure 2. Stress-thickness vs. thickness measured during growth with pauses. Inset: time evolution during pauses.

This use of interrupted growth enables us to attribute the slope of the stress-thickness to the incremental stress at the surface without the effect of stress changes in the subsurface region of the film. An example of stress-thickness measurements with pauses in which the growth was resumed at the same rate is shown in figure 2. The dotted lines indicate the thickness when the growth was paused; the inset shows the time evolution during the pauses (shaded areas in plot). The discontinuities in the stress-thickness vs. thickness when the growth is resumed correspond to the effect of subsurface grain growth on the film stress.

Figure 3a shows the stress –thickness evolution when an electrodeposited Cu film is grown at different rates after each pause. The growth rate (orange line) is superimposed over the corresponding stress-thickness data (blue line). The corresponding grain size for each of the periods of growth is determined by cross-sectioning the sample as shown in figure 3b. Since the growth history is known, the grain size at different depths in the can be used to determine the corresponding grain size for each sequence of growth at the different rates. We confirmed that the grain size in the lower layers does not change when more layers are added by showing that films grown to different final thicknesses have the same grain size evolution.

This approach enables us for the first time to systematically study the separate effects of the growth rate and the grain size on the incremental stress. a 2-d plot of the stress vs. growth rate and grain size for electrodeposited Cu is shown in figure 4. Results of fitting to the model are shown as the surface in the figure. The plot illustrates several trends with the growth rate and grain size. The steady-state stress at high growth rates is more tensile than for the lower growth rates. However, the predicted dependence of the stress on the growth rate is different for the different grain sizes. At high growth rates, the model predicts that the stress is more tensile for small grain size than for large grain size, due to the

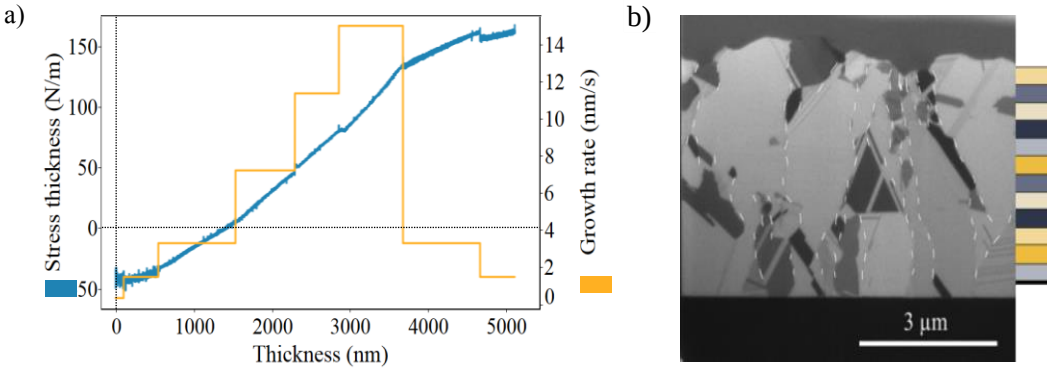

Figure 3. a) Measurements of stress-thickness vs. thickness for electrodeposited Cu at different growth rates (shown by yellow lines). The corresponding incremental stress is determined from the slope of the stress-thickness. b) FIB cross-section used to determine grain size at different thicknesses.

dependence of σ_T on the grain size. However, at low growth rates, there is a crossover in the calculated stress behavior and the stress for the smaller grain size becomes more compressive than the larger grain size. We believe these are the first measurements that have been able to separate the effects of growth rate and grain size at the surface.

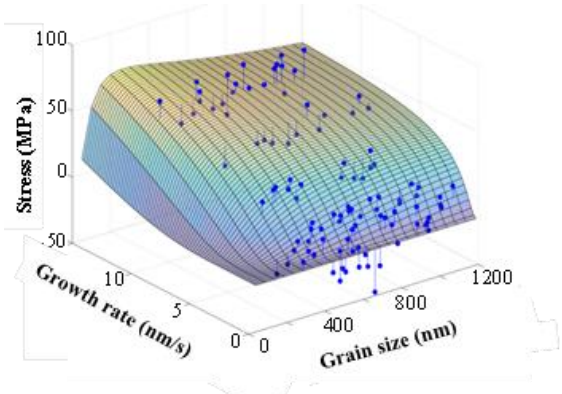

Figure 4. Effect of grain size on steady-state stress vs. growth rate for electrodeposited Cu.

3.3 Effect of electrolyte composition on stress during electrodeposition

The rate of film growth is determined by the net flux of atoms impinging on the surface relative to the flux of atoms leaving the surface. In physical vapor deposition (PVD), the flux of atoms that leaves the surface is usually very small so we can ignore it. However, for electrodeposition there is a significant flux of atoms returning from the surface to the electrolyte. In equilibrium, the flux of atoms onto and off of the surface (called the exchange current) is the same so there is no net deposition. Applying a bias to the sample alters the flux balance away from equilibrium and leads to deposition. To understand how the exchange current and other electrolyte properties alter the surface kinetics during electrodeposition relative to PVD, we performed stress measurements in which the electrolyte was changed systematically.

We measured the stress vs. growth rate in Ni films for different electrolyte compositions and characterized the corresponding grain size. Our results show that changing the sulfamate concentration (in the range from 0.18 to 0.5 M) with a constant boric acid concentration (0.65 M) does not change the stress vs. growth rate behavior within experimental error. However, changing the boric acid concentration (from 0.18 to 0.65 M) while keeping the same sulfamate concentration (0.36 M) leads to a significant difference (as shown in figure 5). The higher acid content has significantly mores tensile stress at the high growth rates which could be due to a change in the interfacial energy driving the grain boundary formation. The mobility parameter (βD_{eff}) obtained from modeling the data is higher for the higher acid content, which may indicate that the atoms are more mobile when the electrolyte is more acidic.

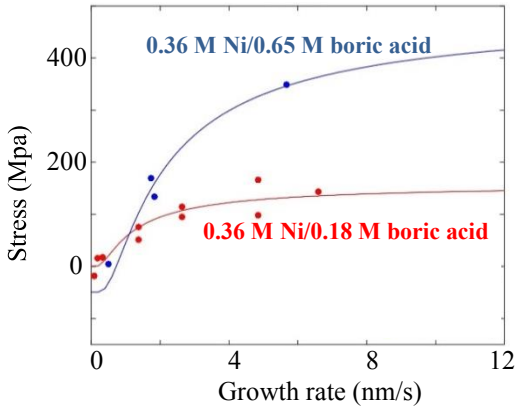

Figure 5. Effect of boric acid concentration in electrolyte on steady-state stress for different growth rates at 300 nm grain size.

We believe this kind of multi-parameter understanding is necessary in order to make a meaningful comparison of the kinetic processes controlling the stress. For example, it lets us separate the grain size effects from the growth rate in the highly tensile electrodeposited Ni. The results give us insight into the fundamentals of the stress-controlling kinetic processes and suggest how the stress can be controlled by changing the electrolyte.

3.4 Extension of growth model to include energetic deposition

The model discussed above only considers non-energetic growth processes. We recently extended this picture to explain stress during sputter deposition by considering additional effects due to the energetic species [15]. The addition of new mechanisms was guided by systematic experimental studies done by the groups of G. Abadias (U. Poitiers) and K. Sarakinos (Linkoping U.) [16, 17] who gave us access to their measurements of stress vs. growth rate, pressure and grain size in sputtered Mo. In

order to derive analytical equations, the model makes simplifying approximations of the complex processes that occur during the interaction of the growing film with energetic particles. Despite these simplifications, we believe that this approach contains enough of the essential physics to provide insight into the processes controlling the evolution of stress in sputtered films.

We proposed two processes suggested by the experimental work and previous models from others (described more fully in the publication); a schematic of the geometry for the additional energetic effects is shown in figure 6. The first mechanism is based on collision-induced densification of the structure near the grain boundary. The shaded area (with width proportional to the implantation depth, *l*) represents the region in which the energetic species enhance incorporation of atoms into the grain boundary (separated by grain size *L*). We consider it to be a diffusion-less process by which atomic collisions within this region knock the atoms into more energetically favorable sites, creating compressive stress (this mechanism was arrived at after considering other diffusion-based mechanisms that give results that are not consistent with the experiments). We model the net effect on the stress by:

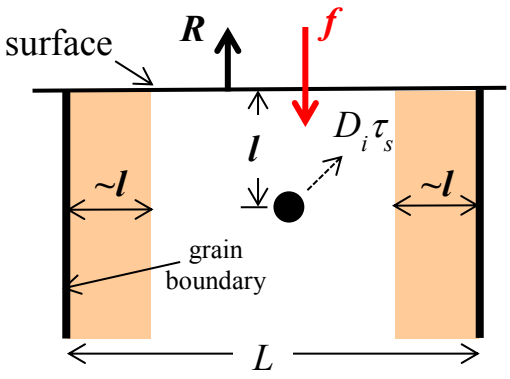

Figure 6. Schematic of stress-inducing processes in model for energetic deposition

$$\sigma_{gb}^{energetic} = A_o * (l/L) \qquad (5)$$

This mechanism is designed to be consistent with studies by Magnfalt et al. [17] that found an inverse grain size dependence of the compressive stress. It is expected to depend on the number of energetic particles per deposited atoms (i.e., the ratio *f/R*). A_o is an adjustable parameter (different for each energy/pressure) that can be used to compare the model with the data.

The second mechanism is due to the introduction of mobile defects in the bulk of the film (i.e., not at the grain boundary), sometimes referred to as subplantation [18]. As shown in figure 6, we assume that a defect (black circle) is created at a depth *l* from the surface. This depth depends on the energy of the incoming particle (sputtered atoms, backscattered gas neutrals or accelerated ions) which is in turn determined by the material system and working gas pressure in the chamber. The resulting defect has a diffusivity D_i and the rate of defect creation is proportional to the flux of energetic particles, *f*. A key element of the model is that the surface is moving upward at a rate *R* due to deposition.

Defect creation is an inherent part of other models, but we have also included the subsequent kinetics of defect annihilation at the surface. In the steady-state regime (i.e., $dC/dt = 0$), the concentration of defects in the film is given by

$$C_{ss} = \frac{c_o f}{R} \frac{1}{\left(1 + \frac{l}{R\tau_s}\right)} \qquad (6)$$

This result is obtained by balancing the rate of defect creation with the rate of annihilation at the surface. c_o is the number of defects produced per energetic particle. τ_s is the characteristic time to diffuse to the surface that is moving upwards at a rate R, given by solving $\sqrt{D_i\tau_s} = l + R\tau_s$. Defects that do not escape to the surface in this time are assumed to become trapped in the layer (in the form of self-interstitials, clusters or dislocation loops). The resulting stress is assumed to be proportional to the concentration of

trapped defects: $\sigma_{bulk}^{energetic} = (1-\frac{l}{L})\,\sigma_o C_{SS}$ where σ_o represents the stress per retained defect. The factor (*1-l/L*) is present because we assume the bulk stress effect is proportional to the fraction of energetic particles that are not within a distance *l* of the grain boundary.

Putting these terms together gives an equation for the steady-state stress during deposition with energetic species:

$$\sigma_{ss}^{sputt} = \sigma_{ss}^{growth} + \sigma_{gb}^{energetic} + \sigma_{bulk}^{energetic} \qquad (7a)$$

$$\sigma_{ss}^{sputt} = \left[\sigma_C + (\sigma_T - \sigma_C)e^{-\frac{\beta D}{RL}}\right] + A_o(l/L) + (1-\frac{l}{L})\frac{B_o}{\left(1+\frac{l}{R\tau_s}\right)} \qquad (7b)$$

where $\sigma_o c_o\, f/R$ is replaced with a single parameter B_o. The predicted stress depends on multiple processing and microstructural parameters (i.e., growth rate, defect flux, temperature, diffusivity of atoms and defects, grain size, defect flux, implantation depth) that enable it to be applied to a wide range of conditions. The different dependence of the individual terms on these parameters shows why the behavior seen in the experiments can be quite complex. It also makes it clear why systematic experiments, in which only a limited number of parameters are changed, are needed to develop a deeper understanding.

This model was used to analyze measurements of stress in sputter-deposited Mo [15] (shown in figure 7) in which the pressure and the growth rate are varied. For each growth rate, the experiments indicate that the stress is more compressive for the lower sputtering pressure (which corresponds to higher particle energy). For each pressure, the stress becomes less tensile/more compressive for higher growth rates. Note that this growth rate dependence is different than for non-energetic deposition where the stress typically becomes more tensile at higher growth rate. The measured average grain size (51 nm) was the same for all the films.

The solid lines in the figure represent the results of fitting the data to the form in eq. 7 [15]. Non-linear least squares fitting was used to obtain a single set of model parameters to explain all the data simultaneously. One value of each of the parameters σ_T, σ_C,βD_{eff} and D_i was used in the fitting for all the pressures and growth rates while A_o,B_o and *l* were given a linear dependence on the pressure to approximate their expected dependence on the particle energy. The good agreement between the model and data suggests that the model is able to capture both the growth rate and the pressure dependence of the stress. Importantly, the energetic terms in the model are able to explain the observed growth rate dependence which is not explained by the growth model alone. The model was also able to explain measurements of the grain size dependence of the stress during HiPIMS deposition.

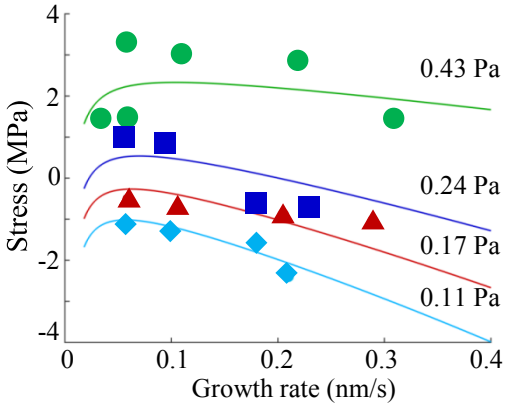

Figure 7. Measurements of steady-state stress vs. growth rate and pressure for Mo deposited by sputtering . The solid lines are fits to the energetic growth model.

3.5 Effect of grain growth on stress evolution

The grain size affects stress in two ways: (1) the changing grain size at the surface modifies the growth stress and (2) grain growth in the layers below the surface can directly induce stress [19, 20]. As

discussed in sec. 3.2, in electrodeposited Cu the grain size changes relatively slowly during growth. Therefore we were able to measure the stress during short intervals of growth to obtain the data at a nearly constant grain size. The corresponding grain size was able to be determined after the growth by measuring it in cross-section at different heights corresponding to the different growth rates.

However, for materials with higher atomic mobility, the grain size changes more rapidly with the thickness so this approach does not work. An example of this is shown from the stress-thickness evolution in evaporated Ni by Yu and Thompson [20] for different growth rates (measurements shown as green lines in Fig. 8) . The slope of the stress-thickness never reaches a constant value even after the film has coalesced into a continuous film. The corresponding grain size was measured to change linearly with the thickness throughout the thickness of the film (zone II in Thornton's structure zone model description). The grain growth was found to depend primarily on the thickness and was essentially the same for different temperatures and growth rates.

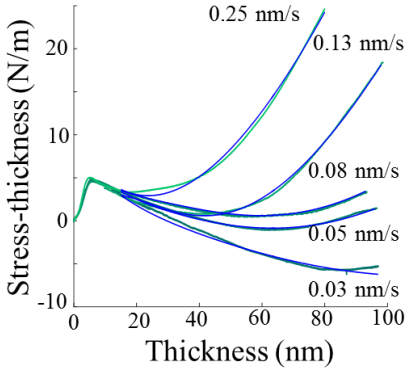

Fig. 8. a) Stress-thickness in evaporated Ni (green line). Blue lines are fit to model described in text.

We explained the continuous change in the slope in terms of the effect of a changing grain size and the stress induced by grain growth. The effect of grain size on the incremental stress in new layers has already been captured in eq. 4 in the terms that depend on *L*. However, when significant subsurface grain growth occurs during deposition, an additional term needs to be added. For growth in Thorton's zone II, the grains are columnar but the grain size increases with film thickness [21]. Chaudhari has described a model in which such grain growth causes the film to shrink due to the elimination of low-density grain boundaries [19]. Since the film is attached to the substrate, this leads to tensile stress. Following this approach [19, 20], we can model the additional stress from the grain growth at each height *z* above the film/substrate interface to be

$$\sigma_{gg}(z) = M_f \Delta a \left(\frac{1}{L_o(z)} - \frac{1}{L_h(z)}\right) \qquad (8)$$

where $L_o(z)$ is the grain size at the time when that layer was deposited, i.e., when the thickness of the film was equal to *z* and $L_h(z)$ is the grain size at the same height when the film has been grown to have a thickness *h*. Δa is related to the density change associated with removing a grain boundary which now allows the stress-thickness ($\bar{\sigma}_{gg} h$) to be calculated by integrating over the film thickness. If we assume that the grain size changes linearly with the thickness (i.e. $L_h(h) = L_o + \alpha h$), then the contribution of grain growth to the slope of the stress-thickness can be shown to be

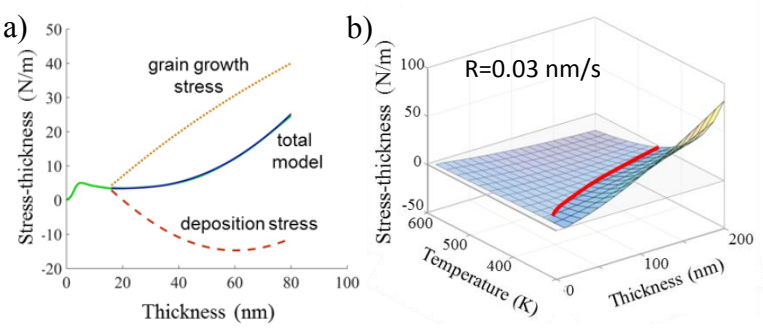

Fig. 9. a) Stress-thickness in evaporated Ni (green line). Total model (blue) is sum of grain growth and deposition stress. b) Model calculation for stress-thickness vs. temperature and thickness.

$$\frac{d(\bar{\sigma}_{gg}h)}{dh} = \frac{\alpha h}{(L_o+\alpha h)^2} \qquad (9)$$

The effects of stress due to both deposition (σ_{growth} in eq. 4) and grain growth ($\bar{\sigma}_{gg}$ in eq. 9) can then be used to explain the changing slope of the stress-thickness. Using Yu and Thompson's data [20] of the grain size vs. thickness, we can calculate their separate contributions (labeled "deposition stress" and "grain growth stress" in Fig. 9(a)). The sum of the two (denoted as "total model") in the same figure is in good agreement with the experimental result plotted by the green line. The total model can then be used to fit the data taken at five different growth rates (shown as the blue lines on Fig. 8) using a single set of the parameters $\sigma_T(L)$, βD_{eff}, Δa, and α and a value of σ_C that depends on the growth rate. The same parameters were also able to fit measurements done at different growth temperatures for a constant growth rate, which allowed us to determine the activation energy for the kinetic processes controlling stress. This work has been written into a manuscript that will be submitted soon; the work will acknowledge support from this DOE program.

The dependence of the stress on deposition conditions and microstructure obtained in this program can be used to tailor the stress profile. As an example, the calculated stress-thickness as a function of thickness and temperature is shown in figure 9(b). The red line shows a cut across the surface that indicates the growth temperature that will keep the stress equal to zero for each thickness and illustrates the predictions our model could provide growers. Additional stress induced by cooling the sample after growth is not shown but could be included.

4. Students and collaborators

The program directly supported the effort of 1 Ph.D. graduate student, Alison Engwall. She successfully defended her thesis in Dec. 2017 and will work as a post-doc at Lawrence Livermore National Labs. In addition, a Sc.M. student (Zhaoxia Rao) participated in the research but was not directly supported by the program. Other Brown Ph.D. students (Fei Pei and Chun-Hao Chen) assisted with the research but received no support. An undergraduate (Chris Miller from U. Colorado) was supported by an NSF REU but contributed to the development of models for this program. Another undergraduate (Mark Karlson, Brown U.) performed modeling of sputtered films.

Other collaborators contributed to the work in this program but received no support. At Brown: Pradeep Guduru , B.W. Sheldon. External: Sean Hearne (Sandia National Labs), L. Ben Freund (UIUC), Gery Stafford (NIST), D. Noel Buckley (U. of Limerick), , Michael Aziz (Harvard U.) K. Sarakinos (Linkoping U.) and G. Abadias (U. of Poitiers).

5. Research Products: Publication and Presentations (total award period)

Publications (17 total: 14 journal, 1 book chapter, 1, Sc.M. thesis, 1 Ph.D. thesis)

1. A.M. Engwall, Z. Rao, E. Chason, "Residual Stress in Electrodeposited Cu Thin Films: Understanding the Combined Effects of Growth Rate and Grain Size", Journal of The Electrochemical Society, 164, D828 (2017).

2. Joseph A. Murphy, Catherine Lenihan, Robert L. Lynch, Eric Chason, and D. Noel Buckley, "In-Situ Measurements of Stress during Electrodeposition of Copper Nanofilms: Effects of Deposition Rate and Grain Size", ECS Transactions 80, 733 (2017).

3. Alison Engwall, Kinetic Modeling of Intrinsic Stress: The Effects of Processing Parameters and Microstructure Evolution, Ph.D. thesis, 2017, Brown University

4. G. Abadias, E. Chason, J. Keckes, M. Sebastiani, G.B. Thompson, E. Barthel, G.L. Doll, C.E. Murray, C.H. Stoessel, L. Martinu, "Stress in thin films and coatings: Current status, challenges and prospects," J. Vac. Sci. Technol., submitted, undergoing final revision

5. Eric Chason, A.M. Engwall and Z. Rao, "Kinetic model for thin film stress including the effect of grain growth," manuscript almost complete (will include acknowledgement to this program)

6. N. K. Mahenderkar, Q. Chen, Y.-C. Liu, A. Duchild, S. Hofheins, E. Chason and J. A. Switzer, "Epitaxial lift-off of electrodeposited single crystal gold foils for flexible electronics," Science 355, 1203 (2017).

7. E. Chason, "Stress measurement in thin films using wafer curvature: principles and applications", in Mechanics of Materials Series: Measurements and Applications, eds. K. Chawla and N. Chawla, Springer, Singapore (2017)

8. A.M. Engwall, Z. Rao and E. Chason, "Origins of residual stress in thin films: interaction between microstructure and growth kinetics", Materials & Design 110, 616 (2016) (Invited contribution to special issue on residual stress), .

9. Z. Rao, Effect of processing conditions on residual stress in electrodeposited nickel thin films, Sc.M. thesis, Brown University 2016

10. Eric Chason and Pradeep Guduru, "Tutorial: Understanding residual stress in polycrystalline thin films through real-time measurements and physical models", J. Appl. Phys.119, 191101 (2016).

11. Eric Chason and Alison M. Engwall, "Relating residual stress to thin film growth processes via a kinetic model and real-time experiments", Thin Solid Films 596 (2015) 2–7

12. E. Chason, M. Karlson, J. Colin, D. Magnfalt, K. Sarakinos, G. Abadias, "A kinetic model for stress generation in thin films grown from energetic vapor fluxes", J. Appl. Phys. 119, 145307 (2016).

13. E. Chason, J.W. Shin, C. –H. Chen, A. Engwall, C. Miller, S.J. Hearne, L.B. Freund, "Growth of patterned island arrays to identify origins of thin film stress," J. Appl. Phys. 115, 123519 (2014).

14. E. Chason, A.M. Engwall, C.M. Miller, C. –H. Chen, A. Bhandari, S.K. Soni, S.J. Hearne, L.B. Freund, B.W. Sheldon, "Stress evolution during growth of 1-d island arrays: kinetics and length scaling," Scripta Mat. 97, 33 (2015)

15. Y. Ishii, C. S. Madi, M.J. Aziz and E. Chason, "Stress evolution in Si during low energy ion bombardment," J. Mater. Res. 24, 2492 (2014)

16. E. Chason, "A kinetic picture of residual stress evolution in polycrystalline thin films", Thin Solid Films 526, 1 (2012).

17. E. Chason, A. Engwal, F. Pei, M. Lafouresse, U. Bertocci, G. Stafford, D. N. Buckley, J. A. Murphy, C. Lenihan, "Understanding residual stress in electrodeposited Cu thin films", J. Electrochemical Soc. 160, D3285 (2013)

Presentations (24 total: 7 invited including keynote and plenary, 9 university/industry, 8 contributed)

Invited international conference

1. E. Chason, Relating thin film stress to the processing conditions and microstructure, 8th Symposium on Functional Coatings and Surface Engineering Montreal, Canada, June 4-7, 2017

2. E. Chason, Z. Rao, and A. Engwall, "Stress in Electrodeposited Ni and Cu: Understanding the Effects of Deposition Conditions and Microstructure," ECS 2017 Washington DC, Oct. 1-4 2017.
3. E. Chason, Trying to Understand Residual Stress in Terms of the Underlying Kinetic Processes (keynote lecture), Joint ICMCTF-SVC Workshop on stress in thin films, Chicago, Oct. 2-5, 2016

4. E. Chason and A. Engwall, Origins of residual stress in thin films: effects of the microstructure and growth kinetics, MS&T, Salt Lake City, Oct. 23-27, 2016

5. E. Chason, Connecting residual stress and thin film growth processes: real-time experiments and a kinetic model (plenary talk), Int'l. Conf. on Metallurgical Coatings and Thin Films (ICMCTF), 4/20/2015, San Diego, CA

6. E. Chason, A kinetic picture for understanding residual stress in thin films: real-time experiments and modeling, Electronic Materials and Applications (EMA), Orland FL, 1/22/2015, Orlando Fl

7. E. Chason, A kinetic model for residual stress evolution in polycrystalline thin films, E-MRS, Strasburg, France, May, 2013

Invited industry/university

1. E. Chason, Origins of residual stress during thin film growth, U. Florida (Gainesville, FL), Sept. 26, 2017

2. E. Chason, Why is there stress in thin films?, U. Alabama (Tuscaloosa, AL), Nov. 10, 2017

3. E. Chason, Residual stress in thin films: real-time experiments and kinetic modeling, Arizona State U., Tempe, AZ 4/25/2014

4. E. Chason, Kinetic Processes Controlling Stress in Thin Films, U. of Limerick, Limerick, Ireland, June, 2014

5. E. Chason, Kinetic Processes Controlling Stress in Thin Films, U. of Linkoping, Linkoping, Sweden, May 14, 2014

6. E. Chason, Understanding residual stress in polycrystalline films: models and experiments, IHPC, Singapore, Oct. 23, 2013

7. E. Chason, Measurement of stress evolution in thin films using real-time in situ wafer curvature, Exhibitors symposium for k-space Assoc. at E-MRS, Strasburg, France, May 2013.

8. E. Chason, Understanding stress evolution in thin films, RPI, Troy, NY, 2/6/2013

9. E. Chason, Understanding stress evolution in thin films, BU seminar, 9/21/2012, Boston MA

Contributed

1. E. Chason, A.M. Engwall, Z. Rao, Residual stress in thin films: effect of processing conditions and microstructure, SVC 2017, Providence RI, April 29-May 4, 2017

2. E. Chason, M. Karlson, J. Colin, D. Magnfalt, K. Sarakinos, G. Abadias, A kinetic model for stress in sputtered thin films, ICMCTF, San Diego, Apr. 24-28, 2016

3. E. Chason, A.M. Engwall, Z. Rao , Residual stress in thin films: effect of growth rate and grain size, TMS meeting, Nashville, TN, Feb, 14-18, 2016

4. A. Engwall, E. Chason, Z. Rao, Chun-Hao Chen, Jae-Wook Shin , Sean Hearne, Noel Buckley, Thin film growth stress from grain boundary formation, MRS, Boston MA, Nov. 29 – Dec. 4, 2015
5. A. Engwall, E. Chason, Chun-Hao Chen, Jae-Wook Shin , Sean Hearne, Noel Buckley, Growth stress in polycrystalline films: the triple junction model from nano- to micro scale, MRS Fall meeting, 12/1/2014, Boston, MA

6. E. Chason, Chun-Hao Chen, Alison Engwal, Jae-Wook Shin , Sean Hearne, L.B. Freund, Model for growth stress in polycrystalline films: comparison with growth on lithographically-patterned and randomly-nucleated films, ICMCTF 5/2014

7. E. Chason, Chun-Hao Chen, Alison Engwall, Jae-Wook Shin , Sean Hearne, Model for growth stress in polycrystalline films, MRS Fall meeting, Boston, MA, Dec. 6, 2013

8. Eric Chason, A kinetic model of stress evolution in thin films, (SES, July 2013, Providence RI).

References cited

1. L. B. Freund and S. Suresh, *Thin Film Materials* Cambridge University Press (2003).

2. E. Chason, *Thin Solid Films*, **526**, 1 (2012).

3. P. Guduru, E. Chason and L. Freund, *Journal of the Mechanics and Physics of Solids*, **51**, 2127 (2003).

4. R. Hoffman, *Thin Solid Films*, **34**, 185 (1976).

5. E. Chason, J. Shin, S. Hearne and L. Freund, *Journal of Applied Physics*, **111**, 083520 (2012).

6. E. Chason, A. Engwall, F. Pei, M. Lafouresse, U. Bertocci, G. Stafford, J. Murphy, C. Lenihan and D. Buckley, *Journal of the Electrochemical Society*, **160**, D3285 (2013).

7. J. W. Shin and E. Chason, *Physical Review Letters*, **103**, 056102 (2009).

8. S. Brankovic, B. Kagajwala, J. George, G. Majkic, G. Stafford and P. Ruchhoeft, *Electrochimica Acta*, **83**, 387 (2012).

9. J. Shin, C. Hangarter, U. Bertocci, Y. Liu, T. Moffat and G. Stafford, *Journal of the Electrochemical Society*, **159**, D479 (2012).

10. O. Kongstein, U. Bertocci and G. Stafford, *Journal of the Electrochemical Society*, **152**, C116 (2005).

11. A. M. Engwall, Z. Rao and E. Chason, *Journal of The Electrochemical Society*, **164**, D828 (2017).

12. A. Engwall, Z. Rao and E. Chason, *Materials & Design*, **110**, 616 (2016).

13. E. Chason, J. W. Shin, C. H. Chen, A. M. Engwall, C. M. Miller, S. J. Hearne and L. B. Freund, *J. Appl. Phys.*, **115**, 123519 (2014).

14. E. Chason, A. M. Engwall, C. M. Miller, C. H. Chen, A. Bhandari, S. K. Soni, S. J. Hearne, L. B. Freund and B. W. Sheldon, *Scripta Mater.*, **97**, 33 (2015).

15. E. Chason, M. Karlson, J. J. Colin, D. Magnfält, K. Sarakinos and G. Abadias, *J. Applied Physics*, **119** (2016).

16. A. Fillon, G. Abadias, A. Michel and C. Jaouen, *Thin Solid Films*, **519**, 1655 (2010).

17. D. Magnfält, G. Abadias and K. Sarakinos, *Appl. Phys. Lett.*, **103**, 051910 (2013).

18. P. Patsalas, C. Gravalidis and S. Logothetidis, *J. Appl. Phys.*, **96**, 6234 (2004).

19. P. Chaudhari, *Journal of Vacuum Science & Technology*, **9**, 520 (1972).

20. H. Z. Yu and C. V. Thompson, *Acta Mater.*, **67**, 189 (2014).

21. J. A. Thornton, *Journal of vacuum Science & Technology*, **11**, 666 (1974).